Electrohydrodynamic Flow Control - A litterature Survey

TOMAS HURTIG, ANDERS LARSSON, MATTIAS LIEFVENDAHL

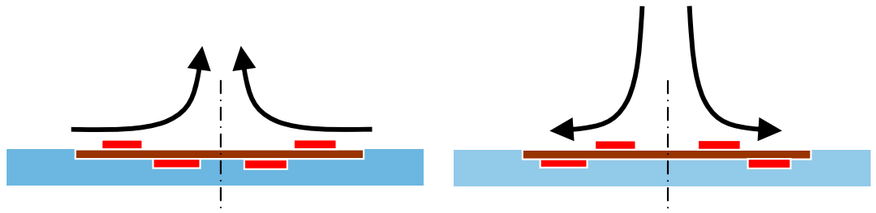

FOI är en huvudsakligen uppdragsfinansierad myndighet under Försvarsdepartementet. Kärnverksamheten är forskning, metod- och teknikutveckling till nytta för försvar och säkerhet. Organisationen har cirka 1000 anställda varav ungefär 800 är forskare. Detta gör organisationen till Sveriges största forskningsinstitut. FOI ger kunderna tillgång till ledande expertis inom ett stort antal tillämpningsområden såsom säkerhetspolitiska studier och analyser inom försvar och säkerhet, bedömning av olika typer av hot, system för ledning och hantering av kriser, skydd mot och hantering av farliga ämnen, IT-säkerhet och nya sensorers möjligheter.

FOI
Totalförsvarets forskningsinstitut
Försvars- och säkerhetssystem
Grindsjöns forskningscentrum
147 25 Tumba

Tel: 08-55 50 30 00
Fax: 08-55 50 31 00

www.foi.se

FOI-R--2417--SE
ISSN 1650-1942

Teknisk rapport
November 2007

Försvars- och säkerhetssystem

Tomas Hurtig, Anders Larsson, Mattias Liefvendahl

Electrohydrodynamic Flow Control - A litterature Survey

Titel	Elektrohydrodynamisk flödeskontroll – En litteraturstudie
Title	Electro hydrodynamic Flow Control – A litterature Survey
Rapportnr/Report no	FOI-R—2417--SE
Rapporttyp Report Type	Teknisk rapport Technical report
Månad/Month	November
Utgivningsår/Year	2007
Antal sidor/Pages	39 p
ISSN	ISSN 1650-1942
Kund/Customer	FMV
Forskningsområde Programme area	5. Bekämpning och skydd 5. Strike and Protection
Delområde Subcategory	55 Flygteknik 55 Aeronautics
Projektnr/Project no	E21201
Godkänd av/Approved by	Torgny Carlsson

FOI, Totalförsvarets Forskningsinstitut	FOI , Swedish Defence Research Agency
Avdelningen för Försvars- och säkerhetssystem	Defence & Security, Systems and Technology
Grindsjöns forskningscentrum	
147 25 Tumba	SE-147 25 Tumba

Table of contents

Sammanfattning

Aerodynamisk flödeskontroll med hjälp av plasmaaktuatorer av den typ som behandlas i denna litteraturöversikt har varit kända sedan tidigt 90-tal och intresset för tekniken har ökat lavinartat de senaste fem åren. Ideér kring användandet av elektriska urladdningar för att påverka chockfronter vid supersoniska och hypersoniska hastigheter har funnits sedan 1960-talet, den typ av yturladding som diskuteras i denna studie är dock betydligt mindre energikrävande och används primärt för att modifiera gränsskikt. Denna liiteraturstudie kring elektrohydrodynamisk flödeskontroll inkluderar experiment, modellering och simuleringsarbeten som publicerats före april 2007.

Nyckelord: flödeskontroll, plasma, elektrohydrodynamik

Summary

The subject of aerodynamic flow control using plasma actuators in the form discussed in this survey originated in the mid 1990s and interest is growing rapidly. Although ideas on how to use an electric discharge to influence the behavior of shock fronts at supersonic speed has been around since the 1960s it is only recently that flow control techniques using surface mounted, relatively low power, actuators has become a major field of research. This litterature survey on the subject of electrohydrodynamic flow control cover experiments, modelling and simulation work published before April 2007.

Keyword: flow control, plasma, electrohydrodynamics

1 Introduction

The subject of aerodynamic flow control using plasma actuators originated in the mid 1990s and interest is growing rapidly. Although ideas on how to use an electric discharge to influence the behaviour of shock fronts at supersonic speed has been around since the 1960s it is only recently that flow control techniques using surface mounted, relatively low power, actuators has become a major field of research. Using the AIAA publication database to search for occurrences of keywords such as ‘plasma actuator’ and ‘plasma flow control’ give a clear indication of a surging interest in this technique, see Table I. Even the pure physics literature is catching on and recently Journal of Physics D: Applied Physics devoted an entire issue to the subject of “Physics and phenomenology of plasma actuators for control of aeronautical flows” [1].

Table 1. Result of keyword search using the AIAA publications database. Note that the search for 2007 only include articles published before 20 April.

Keyword/Year	Plasma actuator	Plasma flow control
2000	0	1
2001	1	1
2002	3	1
2003	15	4
2004	33	9
2005	47	20
2006	82	29
2007 (April)	50	19

It should be noted that the term ‘Plasma flow control’ may refer to any device, from electron guns and very high power plasma sources that ionize the air in front of super velocity or hyper velocity airborne vehicles in order to affect the shape and behavior of the shock front or to guide the flow through a scramjet engine to small, low power, surface mounted plasma generators (actuators) designed to modify the viscous boundary layer by momentum addition. This survey is primarily concerned with the second form of plasma flow control. The study begins with a review of the physics of atmospheric pressure discharges in general and continues with sections on experimental and theoretical (simulation) studies on electrohydrodynamic flow control.

2 Atmospheric pressure discharges

An electrical discharge taking place in air under atmospheric pressure can manifest itself in several forms depending on applied voltage, electrode configuration and other environmental conditions. This chapter will give a concise review of the discharge processes that are relevant for electrohydrodynamic flow control.

2.1 Introduction

The basic mechanism behind an atmospheric pressure discharge is the presence of a free electron that is accelerated in a background electric field. If the field strength is strong enough, the electron will achieve sufficient energy to ionise a gas molecule and thereby liberate another electron. These two electrons are further accelerated and an exponential growth of free electrons occurs. Depending on external conditions (electrode configuration, shape of applied voltage and presence of dielectric barriers) the discharge can manifest itself in several forms. For the case of a dielectric barrier discharge, the discharge can either be filamentary or non-filamentary. The filamentary discharge consists of streamer discharges and the non-filamentary (or diffuse) discharge is a stable and uniform glow discharge. In a dielectric barrier discharge, at least one dielectric barrier is present in the electrode gap. It can either be located in the electrode gap or cover one or both of the electrodes. Both streamers and glow discharges are cold discharges and thus consist of non-equilibrium (or non-thermal) plasmas. In non-equilibrium plasma, the gas temperature (kinetic energy of neutral molecules and ions) are low, whilst the electron temperature is much higher). If there is no dielectric barrier in the electrode gap, the discharges can transit to either spark or arc discharges. These discharges are filamentary and hot discharges.

This chapter gives the basic mechanisms behind atmospheric pressure discharge and concludes with a concise description of discharge types relevant for electrohydrodynamic flow control. The material in this chapter is mainly taken from the Doctoral Thesis by Larsson [2] and the review article by Georghiou [3].

2.2 Fundamental collision processes

The mechanisms that describe the transport and the growth rate of electrons, positive and negative ions, and excited species will be reviewed concisely. A microscopic description of these mechanisms is based on kinetic theory, including the conservation of charge and conservational exchange of momentum and energy between colliding particles. Any collision process between two particles can be defined as follows: if the relative distance between two particles at first decreases and then increases, a collision has occurred if some interaction has changed any physical quantity of the particles involved. When averaged over a sufficient number of individual particles and collisions, a macroscopic (or hydrodynamic) description is obtained. Such a macroscopic description deals with particle densities and collision rates instead of individual particles and collisions, which leads to a simplification of the partial differential equations involved. Thus, in a macroscopic multiparticle picture, the collision process can be characterised in terms of an effective "collision cross-section" (σ) or a "mean free path" (λ), with the relation

$$\sigma = \frac{1}{n\lambda} \qquad (1)$$

where n is the particle number density of the ambient gas. The effective collision cross-section can be interpreted as the cross-sectional area the particle species would have if, in the collision, it behaved as a solid sphere obeying kinetic theory. It should be noted that the collision parameters are dependent on the energy distribution of the particles. The parameters in the macroscopic description are called swarm parameters. To define the mechanisms involved, we divide them into two categories: transport and growth.

Before discussing these two categories, a note regarding elastic and inelastic collisions would be appropriate. An elastic collision is a collision where no kinetic energy is lost by the system. In an inelastic collision, some of the kinetic energy is used for excitation/ionisation. A kinematic study of the system gives the following conclusions. First, when the colliding particles have similar mass, the energy exchange is efficient in elastic collisions, but inefficient in inelastic ones. This means that the exchange of speed is efficient (elastic collision), but the impinging particle can only lose, at most, half of its kinetic energy through excitation, i.e. through increasing the potential energy of the target particle (inelastic collision).

Second, if the impinging particle has a mass much smaller than the target particle, the opposite applies: The energy exchange is inefficient in elastic collisions, but efficient in inelastic ones. This implies that the impinging particle simply bounces off the target and no transfer of kinetic energy occurs (elastic collision), but the impinging particle can lose all its energy in exciting the target (inelastic collision). Hence, electrons are far more efficient than ions in exciting and ionising gas molecules. Further, electrons will not exchange much of their kinetic energy with the neutral molecules, but ions readily do. One consequence of this is that if one has a high electron temperature, the gas temperature will only increase very slowly.

2.2.1 Transport mechanisms

The transport of charged particle discussed in this chapter is relative the background gas.

The drift of charged particles arising from an external field and due to diffusion will be mentioned here. Diffusion is the name given to the spreading out of a species as a result of the chaotic thermal motion of its individual particles. It will eventually result in a uniform density distribution of the particles. The particle flux arising from diffusion is proportional to the particle density gradient, and the constant of proportionality is termed the (thermal) diffusion coefficient. In the presence of an external electric field, the diffusion becomes anisotropic with, effectively, one coefficient parallel and another perpendicular to the field. Further, in a plasma in which there are charged species of both signs, the faster one, generally electrons, tends to diffuse out of the plasma leaving an excess of positive charge, whose space charge field then retards the electrons and accelerates the slow ions, thereby linking their diffusion. This is called ambipolar diffusion.

Consider a charged species in a background of neutral species subjected to an electric field. The drift of one of the charged particles is defined as its net displacement in the direction of the field per unit time, averaged over several mean free paths. The drift velocity of the charged species has, in general, a non-linear relation to the background

electric field strength and the relationship between the drift velocity and the background electric field strength is called mobility. The mobility is defined as the quotient of the drift velocity and the background electric field strength:

$$\mu = v / E \, . \qquad (2)$$

2.2.2 Growth mechanisms

Growth can be either positive or negative and, thus, can involve either a gain or loss in the numbers of a species. The growth mechanisms indicated below include ionisation, excitation, attachment, detachment and recombi¬nation. The charge transfer mechanism is also included. The list is by no means exhaustive, but shows the most important processes occurring in gaseous discharges.

Excitation by electron impact is the most frequent of these processes. Such excitation is the result of transformation of kinetic energy to potential energy in the target molecule without ionisation. Excitations can be classified as either electronic, vibrational, rotational or spin, according to what excitation has been brought about. Electronic excitation is the most important type in gaseous discharges. It involves the transition of an electron situated in one electronic state to another state of higher energy. Another important excited state is the vibrational excitation, which exists for molecules. It is a state where the nuclei oscillate about their positions of equilibrium with, what in a classical sense, would be regarded as simple harmonic motion.

Most electronic excited states are unstable and relax back to the ground state within about 10 ns. However, metastable states exist which have a lifetime of the order of 1 ms. The metastable state is only possible if the excited electron cannot return to the ground state without violating the quantum mechanical selection rules, that is, that two electrons cannot have the same quantum numbers.

As examples, three common excitation processes are represented symbolically by:

$$\begin{aligned} &e + AB \rightarrow AB^{*} + e && \text{(direct excitation)} \\ &e + AB \rightarrow A + B^{*} + e && \text{(dissociative excitation)} \\ &h\nu + AB \rightarrow AB^{*} && \text{(photoexcitation)} \end{aligned}$$

where "e" represents an electron, "AB" a molecular species and * denotes an excited particle. The excitation can be either electronic, vibrational, rotational or spin.

Ionisation by electron impact is the most frequent (gain) process in which positive ions and free electrons are generated. It is caused by inelastic collisions between target molecules and electrons with a kinetic energy above the ionisation potential of the target molecule. Two of the possible processes can be represented symbolically by:

$$\begin{aligned} &e + AB \rightarrow AB^{*} + e && \text{(direct excitation)} \\ &e + AB \rightarrow A + B^{*} + e && \text{(dissociative excitation)} \end{aligned}$$

where "e" represents an electron, "AB" a molecular species and * denotes an excited particle. The excitation can be either electronic, vibrational, rotational or spin.

Ionisation by electron impact is the most frequent (gain) process in which positive ions and free electrons are generated. It is caused by inelastic collisions between target molecules and electrons with a kinetic energy above the ionisation potential of the target molecule. Two of the possible processes can be represented symbolically by:

$$\mathrm{e} + \mathrm{AB} \rightarrow \mathrm{AB}^{+} + 2\mathrm{e} \qquad \text{(direct ionisation)}$$
$$\mathrm{e} + \mathrm{AB} \rightarrow \mathrm{A} + \mathrm{B}^{+} + 2\mathrm{e} \qquad \text{(dissociative ionisation)}$$

Because of the electrostatic forces within the molecule, the ionisation potential for the liberation of a second electron is much higher than for the first ionisation. Hence, doubly ionised molecules are rarely considered within non-thermal discharges, but are present in thermal ones.

Ionisation by photon impact, or photoionisation, is another process whereby positive ions and free electrons are produced. It is of most importance in the streamer propagation process (Section 2.4). The photoionisation can be represented by:

$$h\nu + \mathrm{AB} \rightarrow \mathrm{AB}^{+} + \mathrm{e} \qquad \text{(photoionisation)}$$

The photon does not necessarily need to carry all the energy required for the ionisation. If AB is in an excited state due to a previous photon impact, step photoionisation is possible, especially if AB is in a metastable state.

Attachment is the formation of negative ions by the capture of a free electron. Attachment is only possible if the negative ion has a lower potential energy than the ground state of the capturing molecule. Such capturing molecules are said to be electronegative, whilst the difference in energy between the molecule's ground state and that of the negative ion is called electron affinity. Two possible attachment processes can be represented by:

$$\mathrm{e} + \mathrm{AB} \rightarrow \mathrm{AB}^{-} \qquad \text{(direct attachment)}$$
$$\mathrm{e} + \mathrm{AB} \rightarrow \mathrm{A} + \mathrm{B}^{-} \qquad \text{(dissociative attachment)}$$

No doubly-charged negative ions have been found since no negative ion has been found to be electronegative.

Detachment is the liberation of an electron from a negative ion. It is mostly comprised of collision detachment, i.e., it includes the interaction of a third party. Only three of the many possible detachment processes are presented here:

$$\mathrm{AB}^{-} + \mathrm{C} \rightarrow \mathrm{e} + \mathrm{AB} + \mathrm{C} \qquad \text{(direct detachment)}$$
$$\mathrm{AB}^{-} + \mathrm{C} \rightarrow \mathrm{e} + \mathrm{A} + \mathrm{B} + \mathrm{C} \qquad \text{(dissociative detachment)}$$
$$\mathrm{AB}^{-} + h\nu \rightarrow \mathrm{AB} + \mathrm{e} \qquad \text{(photodetachment)}$$

Recombination happens when a positive ion captures an electron, either a free electron or an electron from a negative ion. The recombination processes can be represented by:

$$\mathrm{e} + \mathrm{CD}^{+} \rightarrow \mathrm{CD} \qquad \text{(electron-ion recombination)}$$
$$\mathrm{AB}^{-} + \mathrm{CD}^{+} \rightarrow \mathrm{AB} + \mathrm{CD} \qquad \text{(ion-ion recombination)}$$

Recombination is the only loss mechanism for positive ions.

Charge transfer is the transfer of charge without changing the number of ions, but by changing the species of ions. Charge transfer is equally applicable to positive and negative ions, but the two examples below are taken from the processes of positive ion charge transfer.

$$AB + CD^+ \rightarrow A + B^+ + CD \text{ (dissociative charge transfer)}$$
$$AB + CD^+ + E \rightarrow AB^+ + CD + E \text{ (three-body charge transfer)}$$

2.3 Reactions and reaction rates in air

In air under normal atmospheric conditions, it is several constituents that take part in the processes outlined in the former section. In fact, more than 40 reacting constituents and more than 250 specific reactions can appear in gas discharges in nitrogen-oxygen mixtures [4]. What follows is just a brief discussion regarding the most important and frequent products of air discharges and the rate at which these products are produced.

2.3.1 Air discharge reactions and their products

Free electrons are mainly produced by direct ionisation according to the following reactions:

$$e + N_2 \rightarrow N_2^+ + 2e \quad (3)$$
$$e + O_2 \rightarrow O_2^+ + 2e \quad (4)$$

Dissociative ionisation is less frequent, partly due to the higher energy needed. Free electrons are also produced by collisional detachment

$$O_x^- + M \rightarrow O_x + M + e \quad (5)$$

where x can be 1, 2 or 3 and M an oxygen or a nitrogen molecule. Finally, photoionisation can also occur.
The most important positive ions are the nitrogen ions and , and the oxygen ion . They are either generated by direct ionisation or by indirect ionisation involving cascade reactions, e.g.,

$$e + N_2 \rightarrow N_2^* + e;\ N_2^* + N_2 \rightarrow N_4^+ + e \quad (6)$$
$$e + N_2 \rightarrow N_2^+ + 2e;\ N_2^+ + 2N_2 \rightarrow N_4^+ + N_2 \quad (7)$$

Negative ions are produced by attachment. Since no stable nitrogen negative ions have been detected in nitrogen and air, the most common negative ions are the oxygen ions for x = 1, 2, or 3. Under the conditions of interest in breakdown studies, the attachment mechanism is the dissociative attachment reaction:

. $$e + O_2 \rightarrow O^- + O \quad (8)$$

The negative ion thus formed reacts with oxygen molecules to produce O_2^- and O_3^-.

2.3.2 Influence of water vapour

The dominant positive ion in corona discharges in the presence of water vapour is the oxonium ion H3O+ together with its hydrates H3O+(H2O)n, where n is the number of water molecules in the cluster. Two cascade reactions producing hydronium ions are suggested:

$$N_2^+ + H_2O \rightarrow N_2H^+ + OH;\ N_2H^+ + H_2O \rightarrow H_3O^+ + N_2 \quad (9)$$

$$N_2^+ + H_2O \rightarrow N_2 + H_2O^+;\ H_2O^+ + H_2O \rightarrow H_3O^+ + OH \quad (10)$$

where the first one is believed to be predominant. Cluster conglomerates with n as high as 7 have been found for an absolute humidity of 5 g/m3 under atmospheric conditions. With a lower humidity, the most common complex appears at n = 3.

Electrons are not attached to water molecules and the most promi¬nent effect that water vapour has on negative ions arises in the cluster formation:

$$O_2^-(H_2O)_{n-1} + H_2O \rightarrow O_2^-(H_2O)_n \quad (11)$$

where clusters with n > 3 are unlikely to be found because the production rate is very small. Declustering, i.e., the reverse of (11), is also an important process.

Water molecules are efficient at absorbing photons and they have an ionisation energy that are lower than the ones for oxygen and nitrogen.

2.3.3 Reaction rates for discharge simulations

The coefficients appearing in Bolzmann's equations for the electrons and ions are the transport coefficients (for mobility and diffusion) and the rate coefficients (for ionisation, attachment, detachment, recombination and excitation). The transport coefficients have already been mentioned in Section 2.2.1. The rate coefficients give the gain or loss of a species per unit length. In principle, a rate coefficient should exist for each of the individual reactions but for practical reasons, an average coefficient represents all the reactions in most applications. For instance, the ionisation coefficient α is defined by the average number of ionisations per unit length in the direction of the electric field. Thus, it is equal to the number of new electrons, so that

. $$\alpha = \frac{\text{number of new free electrons}}{\text{unit length}} \quad (12)$$

Similar definitions are given for the other rate coefficients. In fact, for this definition of α the detachment is also included. In attaching (i.e., electronegative) gases, the effective ionisation coefficient α_{eff} is often used. This is defined as the ionisation α minus the attachment η, i.e.,

$$\alpha_{\text{eff}} = \alpha - \eta \quad (13)$$

which is the net number of new free electrons per unit length. The electrical breakdown condition implies a net production of free electrons, i.e., that the effective ionisation coefficient is greater than zero. This coefficient is strongly dependent on the ambient electric field strength and, in air at standard atmospheric pressure and temperature (i.e., p_0 = 1,013 bar = 1013 hPa and T_0 = 20 °C = 293 K), the electric field strength for which $\alpha_{eff} = 0$ is 2,6 MV/m. For non-standard atmospheric conditions, the electric field strength should be multiplied by the relative air density correction factor δ, given by:

$$\delta = \left(\frac{p}{p_0} \right) \left(\frac{273 + T_0}{273 + T} \right) \qquad (14)$$

where T and T_0 are given in degrees Celsius.

As mentioned above, the ionisation and attachment coefficients are not constant and are often expressed as a function of the reduced field, i.e., the electric field divided by the gas density. As an example, the reduced ionisation coefficient is expressed as α/N = f(E/N). Such a relationship is typical for two-body processes. The rate coefficients expressed in this way are integrated quantities that include all the possible reactions. This kind of data is called swarm data and is only valid when the number of particles is sufficiently large. The swarm conditions are not fulfilled in the early stage of a single electron avalanche, but they are in most other cases relevant to discharges in air under atmospheric conditions.

Several compilations of reaction rates exist, but one ought to take the data from original papers to be sure that it is appropriate for the study.

2.4 The streamer and the glow discharges

2.4.1 Seeding electrons

To initiate a discharge at least one seeding electron is needed. There is a natural production of free electrons caused by cosmic rays and natural radiation at a rate of the order of 10^7 $m^{-3}s^{-1}$, where the natural radiation is that prevailing at sea level. These free electrons lives for about 10 ns before they are attached to the negative oxygen molecule and form a negative ion. However, this production rate and life time is not sufficient to explain the the time-lag between when the electric field strength is high enough to accelerate a free electron to the ionisation potential and the time when the first discharge event actually occurs (the statistical time-lag). For discharges in air under atmospheric conditions the detachment of negative oxygen ions as a source of seeding electrons is important. In the presence of water vapour, clustering effects must be taken into account.

Free electrons can also be generated by external sources, e.g., by subjecting the electrode gap to UV-irradiation or an ionising laser pulse.

2.4.2 Electron avalanches, streamers and glow

The multiplication of free electrons creates an electron avalanche. If the external field exceeds the field needed to accelerate the electrons to the ionisation energy, the number of electrons in this electron avalanche grows exponentially according to

$$N_e(x) = N_{e0} \exp\left(\int_0^x \alpha_{\text{eff}} \, dx'\right) \qquad (15)$$

in the opposite direction to the background electric field. Here x is the length of the avalanche and N_{e0} the initial number of electrons. These electrons spread out radially by diffusion such that the radius of diffusion r_D is given by:

$$r_D = \left(\frac{4Dx}{v_e}\right)^{1/2} \qquad (16)$$

where v_e is the drift velocity of electrons in the (opposite) direction of the electric field, which gives the avalanche the shape of a rotational paraboloid. It has been experimentally proven that, when the avalanche grows to about 108 electrons, the space charge in the avalanche tip creates an electric field that significantly adds to the background electric field distribution in the vicinity of its tip. New avalanches can be initiated along the tail of the first one and are directed towards its tip (Figure 2.1). This avalanche-to-streamer transition has been observed when the product of the pressure and the electrode spacing (pd) exceeds about 5 mm· bar (500 m· Pa) for a uniform applied electric field. For a non-uniform electric field, the critical pd-value for the avalanche-to-streamer transition is even lower. Below this limit, the space-charge does not significantly influence the discharge and a transition to a filamentary discharge does not occur. In such a case, a diffuse, non-filamentary glow discharge can take place.

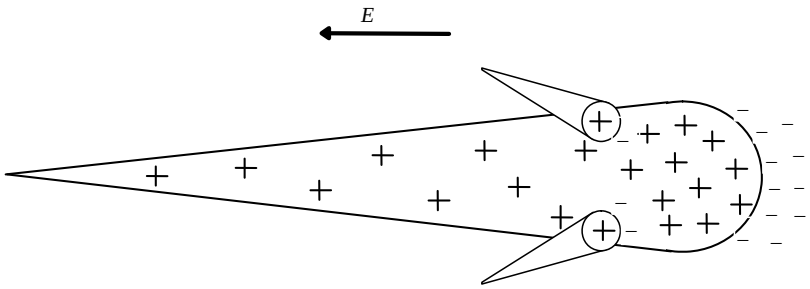

Figure 2.1. The first avalanche with the subsequent generation of successive avalanches.

A schematic representation of the cathode-directed (positive) streamer propagation is outlined in Fig. 2.2. In a timescale upon which the electrons move but the positive ions are stationary, the positive streamer inception and propagation can be described as follows: Free seeding electrons are mainly created by the detachment of oxygen ions, whereupon they are accelerated in the applied background electric field (Figure 2.2a). The electrons are accelerated towards the anode in the applied field. In transit, collisions take place with the gas molecules and excitations and ionisations occur, thereby creating an electron avalanche (Figure 2.2b). The avalanche electrons continue to ionise and excite the molecules until they reach the anode where they are collected. Recombinations and de-excitations occur in the avalanche tail, leading to the emission of photons. Some of these photons will ionise molecules in the vicinity of the avalanche (Figure 2.2c). If the space-charge field from the avalanche is high enough, the newly created free electrons form further avalanches that are directed towards the space-charge centre of the first one (Figure 2.2d). The electrons in the second generation of avalanches neutralise

the positive charge in the first avalanche, then the second generation avalanches radiate photons causing additional photo-ionisation. This rough picture gives, prima facie, that a positive streamer is equivalent to a sudden injection of negative charge into the anode at the streamer inception, followed by an apparent drift of positive charge into the gap with a drift velocity equal to the streamer velocity. Only one of the second generation avalanches is shown in Figure 2.2, but many of them will occur.

A typical streamer current measured at the anode will have a rise time of about 10–50 ns and an almost exponential tail with a decay time of about 200-500 ns. If the streamer is confined in a short gap, the duration of the current will be shorter (Fig. 2.4). The shape of the current impulse is remarkably independent of whether a single streamer, a branched streamer or multiple streamers are present, but the amplitude of the current impulse varies considerably for different cases, ranging from milliamperes up to several amperes. The light emitted from a streamer originates from the recombinations and de-excitations which occur at the streamer head. Thus still photographs of streamers show a diffuse track caused by light emitted almost solely from the streamer front.

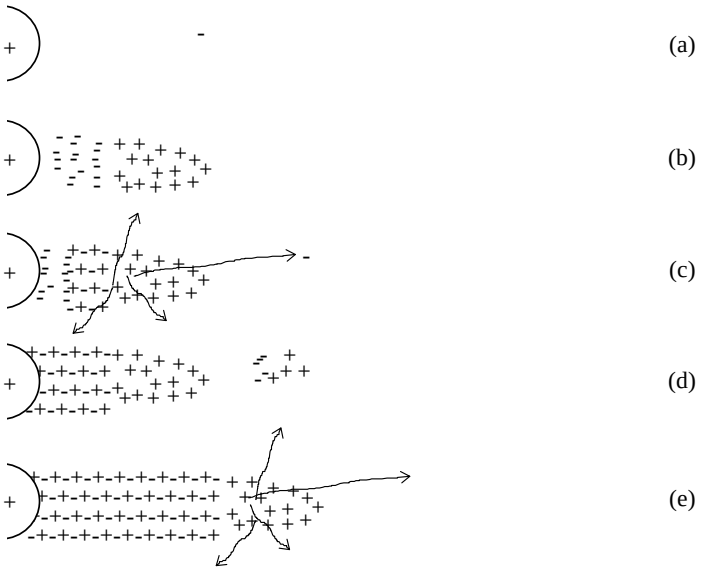

Figure 2.2. Positive streamer inception and propagation (schematic).

2.5 Transition to spark and arc discharges

If there is no dielectric barrier that hinders the current from flowing in the discharge, the cold discharge will be transited into a hot one. If the applied voltage is pulsed, then the cold discharge will be transited into a transient spark discharge. If the applied voltage source can deliver electric energy continuously, the cold discharge will be transited into a stable arc discharge.

2.6 Modelling of non-thermal plasmas

A significant amount of work, including theoretical, numerical and experimental, has been devoted to the understanding the growth of electron avalanches, their transition into streamers, streamer propagation and glow discharges, as these constitute the main mechanisms for non-thermal plasma production at atmospheric pressure. The subsequent transition into spark or arc discharges will shortly be discussed in the following section.

The most frequent modelling approach of streamer and glow discharges are based on hydrodynamic diffusion-drift approximation models to simulate the evolution of charge densities, although kinetic models are less approximate. The main reason for this is that the kinetic simulations are extremely time consuming. The simplest hydrodynamic model that still is able to simulate cold gaseous discharges is the continuity equations for the involved charge carriers coupled with Poisson's equation. The minimum set of charge carriers are the electrons, positive and negative ions. The continuity equations for these species are given by

$$\frac{\partial n_\mathrm{e}}{\partial t} = \alpha \nu_\mathrm{e} n_\mathrm{e} - \eta \nu_\mathrm{e} n_\mathrm{e} - \beta_\mathrm{ep} n_\mathrm{p} n_\mathrm{e} - \nabla \cdot \left(\boldsymbol{\nu}_\mathrm{e} n_\mathrm{e} - \boldsymbol{D}_\mathrm{e} \nabla n_\mathrm{e} \right) + S \tag{17}$$

$$\frac{\partial n_\mathrm{p}}{\partial t} = \alpha \nu_\mathrm{e} n_\mathrm{e} - \beta_\mathrm{ep} n_\mathrm{p} n_\mathrm{e} - \beta_\mathrm{np} n_\mathrm{n} n_\mathrm{p} - \nabla \cdot \left(\boldsymbol{\nu}_\mathrm{p} n_\mathrm{p} \right) + S \tag{18}$$

$$\frac{\partial n_\mathrm{n}}{\partial t} = \eta \nu_\mathrm{e} n_\mathrm{e} - \beta_\mathrm{np} n_\mathrm{n} n_\mathrm{p} - \nabla \cdot \left(\boldsymbol{\nu}_\mathrm{n} n_\mathrm{n} \right) \tag{19}$$

where t is the time, n_e, n_p and n_n are charge densities for electrons, positive ions and negative ions, $|\boldsymbol{\nu}_\mathrm{e}| = \nu_\mathrm{e}$, $|\boldsymbol{\nu}_\mathrm{p}| = \nu_\mathrm{p}$ and $|\boldsymbol{\nu}_\mathrm{n}| = \nu_\mathrm{n}$ are the drift velocities for electrons, positive and negative ions, $\boldsymbol{D}_\mathrm{e}$ is the electron diffusion coefficient and S is the source term due to photo-ionisation. The coefficients α, η, β_ep, β_np denote the ionisation, the attachment, the electron-positive-ion recombination and the negative-ion-positive-ion recombination, respectively.

Poisson's equation is given by

$$\nabla \cdot \left(\varepsilon_0 \nabla V \right) = -e \cdot \left(n_p - n_n - n_e \right) \tag{20}$$

where ε_0 is the permittivity of free space, e is the electron charge and V is the electric potential. The electric field $\boldsymbol{E}$ is given by

$$\boldsymbol{E} = -\nabla V \tag{21}$$

The equations are closed in the following manner. The coefficients α, η, β_ep, β_np and D_e are taken from either experiments or kinetic model simulations, where the former are most common. The photo-ionisation source S of electrons and positive ions is the most difficult component to model with sufficient accuracy since it is a non-local quantity. Regarding the velocities, instead of introducing a momentum balance equation, the electron and ions velocities are assumed to be related to the electric field strength according to

$$\nu_\mathrm{e} = \mu_\mathrm{e} \cdot E \,;\; \nu_\mathrm{p} = \mu_\mathrm{p} \cdot E \,;\; \nu_\mathrm{n} = \mu_\mathrm{n} \cdot E \tag{22}$$

where the coefficients of mobility μ are taken from experiments. None of these coefficients are constant; they are dependent on the electric field strength E and the gas density n and in most cases the reduced electric field strength E/n. A historical note: In older literature, the pressure p instead of the density n is given. Physically, the gas density is the correct quantity, but the pressure is easer to measure. To get the correct relations, the pressure must be corrected for the temperature.

Models such as described above have been used in successful simulations of discharge behaviour. They are in a vast majority of cases carried out through the finite difference (FD) method together with the flux-corrected transport (FCT) technique where the domain of interest is split into structured grids, even if finite elements coupled to the FCT has also been presented. However, the model incorporates several assumptions, which may not be valid for the particular use of interest.

- The ionisation degree is considered being so low that the density of the background gas n is not significantly reduced by the ionisation processes. This is a valid assumption for cold discharges. When the ionisation degree becomes too high, coulomb collisions between electrons and positive ions starts to be efficient and the discharge starts to get hot.
- The diffusion of positive and negative ions is neglected. This assumption must be carefully considered in glow discharges.
- The model requires a significant amount of experimentally achieved coefficients. The justification of the values of these coefficients is tricky.
- The electromagnetic equations are reduced to Poisson's equation. This is valid if the currents are small enough to create negligible magnetic fields. This is true in cold discharges.
- The different species are bunched together to being either electrons, positive or negative ions. Depending on the application, the chemistry must be expanded, which implies that each individual species must have its own continuity equation.
- A single-moment model is used, using the continuity equation for the involved species. The momentum and energy equilibrium times are generally small compared to any macroscopic scale variation of the system. It has been shown that this is the case for reduced electric field strengths of 1500 Td ($1\ \mathrm{Td} = 10^{-21}\ \mathrm{Vm}^2$) or 38 MV/m at atmospheric pressure and a temperature of 20ºC.
- There is a limit upon the upper frequency of the applied voltage. The electron collision frequency must be sufficient high for the electrons to achieve the appropriate energy distribution corresponding to the momentary electric field strength. The relaxation time for the energy distribution is of the order of 10^{-11} s, which is a short time for voltage variations in the megahertz range.

And finally, all electrode or barrier effects such as electron emission, electrode sheaths and charging of barriers must be treated by specific models or as boundary conditions.

2.7 Dielectric barrier discharges

The purpose of introducing a barrier in the discharge is to prevent a disruptive discharge, that is, to prevent the creation of an arc or a spark discharge that short-circuits the electrode gap. The barriers are normally introduced as a dielectric layer at the electrodes. The process of a dielectric barrier discharge is as follows. When the voltage is applied and the electric field in the air E_{air} is strong enough to start ionisation, positive and

negative ions are formed in the air gap. The ions migrate in the electric field towards the electrodes. But since the electrodes are covered by dielectric materials, the electric charge of the ions cannot be transferred to the electrodes, but are stuck on the electrode surface. Thus, there is a charge accumulation on both of the dielectric layers. The surface charge has the following effect on the electric field strength in the configuration: The electric field strength in air E_{air} is reduced and the electric field strength in the barriers $E_{barrier}$ is increased. E_{air} is reduced until the field strength in the air is below the threshold for gas breakdown. This situation is illustrated in Figure 2.3 where $E_{barrier} > E_{air}$. The field strength in air is not high enough to create any new ions and the electric field in the barriers are not strong enough to cause a dielectric failure of the barrier. Thus, the situation is stable without any discharge. However, if the applied voltage is alternating, the voltage will reverse and the new conditions will be favourable for a new series of ionisations and charge accumulations with negative charge on the lower electrode and positive charge at the upper electrode. If the frequency of the alternating voltage is sufficiently high, the charge accumulation on the dielectric surfaces will not be enough to reduce the field strength in the air gap to be below the threshold for gas breakdown.

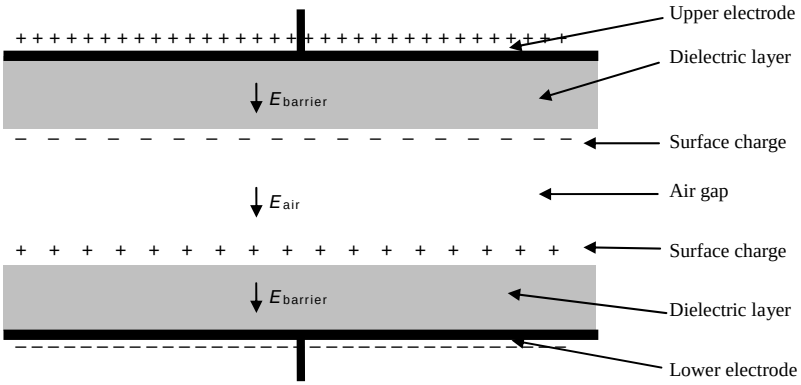

Figure 2.3. Typical configuration of a dielectric barrier discharge where both electrodes are covered with a dielectric layer. The figure is not to scale; normally, the dielectric layers are much thinner than the air-gap.

3 Plasma flow control using AC discharges

Although many different varieties exist, the term ‘plasma actuator’ usually refers to a surface mounted device powered by an alternating current (AC) at a few kilohertz (3-10 kHz) and a few kilovolts (4-10 kV). The actuator is composed of two strip electrodes (wires or foils) one of which is embedded in a dielectric and the other exposed to the surrounding medium, usually air, see Figure 3.1. The width of the electrodes is typically of the order of centimetre, and the thickness of the order of 0,1 mm. The actuator can be given any length in the direction normal to the paper and the power required to drive the discharge varies between 10 W/m up to 1 kW/m depending on the mode in which it is operating.

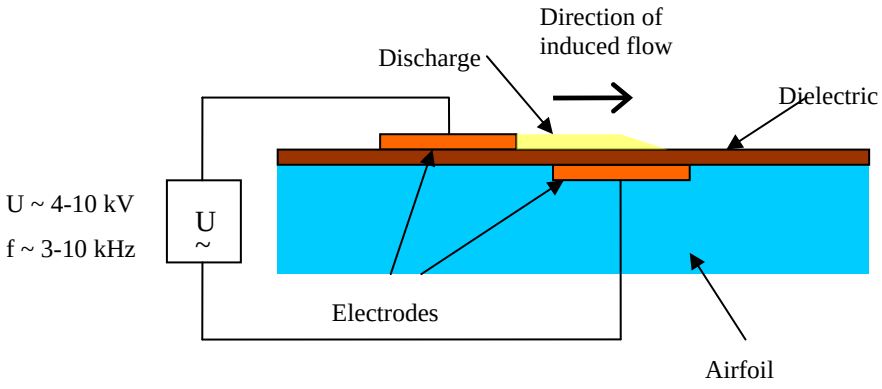

Figure 3.1. Typical geometry of surface mounted plasma actuator. The width of the electrodes is usually of the order of centimetre, and the thickness of the order of 0.1 mm. The actuator can be given any length in the direction normal to the paper and the power required to drive the discharge varies between 10 W/m up to 1 kW/m depending on the mode in which it is operating.

The induced flow velocity is typically about 3 m/s, although some researchers report velocities up to 10 m/s and the power to thrust conversion factor is about 1 mN/W. In laboratory setups the electrodes are usually made up of conducting tape or foil, usually copper tape and the dielectric is usually Kapton™ Polyimide tape or foil [5-10]. A more aerodynamically sound setup would be to have the top electrode recessed into the dielectric as drawn in Figure 3.2. Another way of minimizing the protrusion of the electrode into the boundary layer flow would be to sputter or to use vapour deposition to deposit a very thin layer of electrode material on a dielectric surface [9].

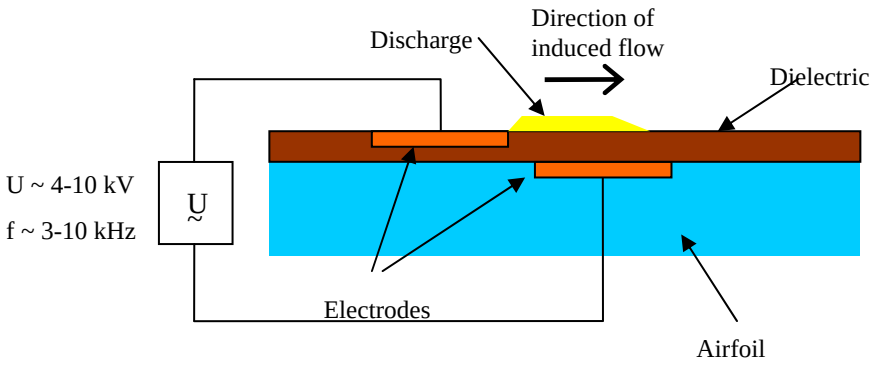

Figure 3.2. A more aerodynamically sound version of the actuator in Figure 3.1. Here the top electrode has been recessed into the dielectric in order not to interfere with the boundary layer flow.

Plasma actuators modify the boundary flow by adding momentum, not mass. The efficiency of the plasma actuator is maximized by minimizing the energy lost in poor impedance matching, dielectric heating and ionization. The power flow in a plasma actuator is illustrated in Figure 3.3.

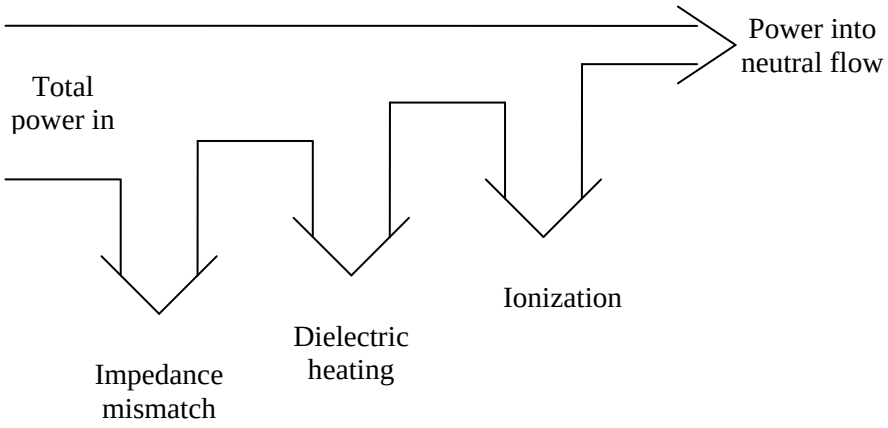

Figure 3.3. Illustration of power flow in a plasma actuator. Losses due to impedance mismatch are minimized by matching the driving circuit to the plasma actuator. Losses due to dielectric heating are minimized by using small volumes of dielectric with low loss. The cost of ionization is reduced by choosing the correct mode of operation (frequency and applied voltage).

The impedance mismatch stems from the fact that the plasma actuator is a highly capacitive load and it can be compensated for by introducing an impedance matching network. In its simplest form the impedance matching network can consist of a RLC circuit placed in parallel to the plasma actuator [11]. A typical example of an impedance matching network can be seen in Figure 3.4.

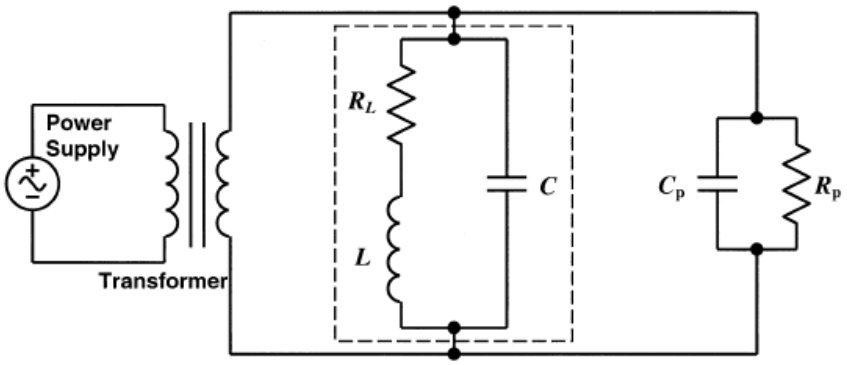

Figure 3.4. Schematic picture of experimental setup including an impedance matching network [11]. The plasma actuator is represented by a parallel RC circuit and the impedance matching network is marked by the dotted line.

Dielectric heating is minimized by choosing a low loss dielectric, see Section 3.2.1. Since the plasma actuator needs a plasma to operate it is impossible to eliminate the losses due to ionization but by operating the actuator in the correct mode it is possible to minimize the cost (in terms of energy) per electron-ion pair produced. There are different ideas on how to accomplish this but J. Reece Roth seems to have come up with one possible solution which he calls the One Atmosphere Uniform Glow Discharge Plasma (OAUGDP) [12]. In this mode of operation the voltage and the frequency of the discharge are chosen so that electrons have time to move between the electrodes in one period. Ions on the other hand do not have time to move between the electrodes (due to their larger mass) and can be considered to be ‘trapped’. This way a very small amount of ions will be absorbed by the electrodes. The minimum amount of energy required to create an electron-ion pair in air under atmospheric pressure is about 81 eV and Roth claims that the OAUGDP does not use more energy than this in continuous mode [13].

3.1 Theory

Early experiments by Roth *et al*. [13] showed that it was possible to use a non-symmetric AC surface discharge to transfer momentum from ions in the plasma to the surrounding air and that the resulting average airflow had a preferred direction related to the asymmetry of the discharge. Note that if a symmetric AC discharge is used one can expect the average momentum transfer to be zero since the direction of the ions change when the applied voltage changes sign. The exact reason for net transfer of momentum in the non-symmetric plasma actuator is not completely understood yet. As mentioned earlier it is the electrons that cause ionization and the ions that transfer momentum from the discharge (plasma) to the surrounding neutral gas. One reason for the net momentum transfer lies in the way the plasma modifies (cancels out) the electric field between the electrodes that is otherwise present when the air between the electrodes is not ionized. Since charged particles in the plasma are free to move they will arrange themselves as to cancel out the electric field in the plasma interior, thermal motion causes this cancellation of the field to be incomplete near the plasma boundaries. The density of ions and electrons (n_i and n_e) can be related to the local plasma potential, V_p, through the Boltzmann equation:

$$n_{i,e} = n_0 \exp\left[\mp (eV_p / kT_{i,e})\right] \approx n_0 \left[1 \mp (eV_p / kT_{i,e})\right] \quad (23)$$

where n_0 is the density of the background plasma, k is Boltzmann's constant and T is the temperature of the particle species. The charge density at any point in the plasma is

$$\rho = e(n_i - n_e) \approx -en_0\left[(eV_p / kT_i) + (eV_p / kT_e)\right] \quad (24)$$

Assuming electrostatic conditions the potential in the plasma can be related to the charge density in the following way

$$-\nabla^2 V_p = \rho / \varepsilon_0 \quad (25)$$

where ε_0 is the permittivity of free space. Combining the above equations we obtain

$$\nabla^2 V_p = (e^2 n_0 / \varepsilon_0)(1/kT_i + 1/kT_e)V_p \quad (26)$$

where

$$1/\lambda_D^2 = (e^2 n_0 / \varepsilon_0)(1/kT_i + 1/kT_e) \quad (27)$$

is usually referred to as the Debye length and is the electrostatic shielding distance in a plasma. We now combine the above results and find a relation between the charge density and the local potential in a plasma

$$\rho = -(\varepsilon_0 / \lambda_D^2)V_p \quad (28)$$

The volumetric force acting on a charge density, ρ, is

$$\mathbf{f} = \rho\mathbf{E} = -(\varepsilon_0 / \lambda_D^2)V_p\mathbf{E} \quad (29)$$

The above equation is not solvable by means of analytical methods in the geometry used for plasma actuators, instead Enloe *et al.* solved Equation 29 in the cylindrically symmetric case of a coaxial system where the potential drop was applied between the inner and outer cylinders. It was found that the difference in radius between inner and outer conductors caused a net force on the plasma ions directed against the inner electrode. The force is restricted to the very small volume around the inner electrode where charge separation occurs, see Figure 3.5.

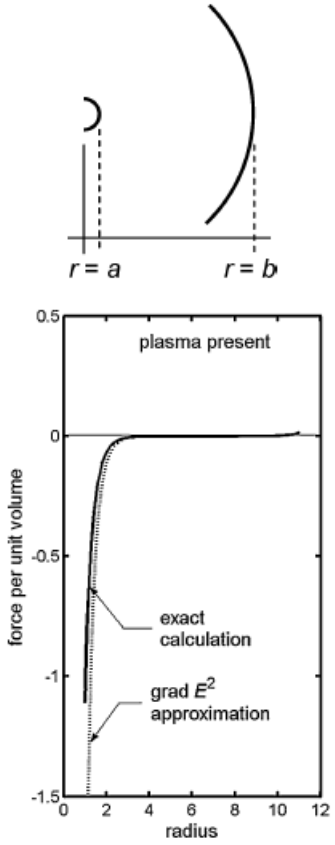

Figure 3.5. Top figure shows coaxial geometry used by Enloe *et al*. when solving Equation 29 analytically. Bottom figure is a graphical representation of the solution. Note how the volume force (curve denoted 'exact solution') increases dramatically close to the inner radius.

Other than the attempts by Enloe *et al*. theory on plasma actuators is very scarce and explanations of the physics involved are usually qualitative and sketchy. It is clear that it is the ions and not the electrons that transfer momentum from the plasma to the surrounding gas and that the asymmetry of the discharge is fundamental for obtaining a net momentum even when an alternating voltage is applied. According to Font *et al*. it is the deposition of electrons on the dielectric during the negative half cycle that 'seeds' the plasma during the positive half cycle [14]. This way the plasma is less dense during the negative half cycle than during the positive half cycle and this would cause more ions to transfer their momentum to the surrounding air during the positive half cycle than during the negative.

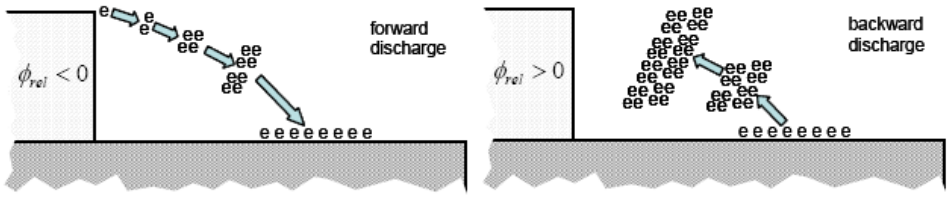

Figure 3.6. Schematic picture of negative half cycle (left, top electrode negative relative to dielectric) and positive half cycle (right, top electrode positive relative to dielectric). Font *et al*. calls the negative half cycle 'forward discharge' since, during this cycle, electrons travel in the direction of fluid flow and the positive half cycle is referred to as 'backward discharge'. It is during the 'backward discharge' that electrons are collected from the dielectric to the top electrode and causes plasma production (and hence ion density) to be higher in this part of the discharge cycle [14].

The influence of negative ions (O-) was investigated by placing the actuator in pure nitrogen that does not produce negative ions and it was found that the efficiency of the actuator was lower than in air [10]. It was also found that the efficiency of the actuator was better in carbon dioxide than in nitrogen, suggesting again that negative ions do have an effect on the performance of the plasma actuator, see Figure 3.7.

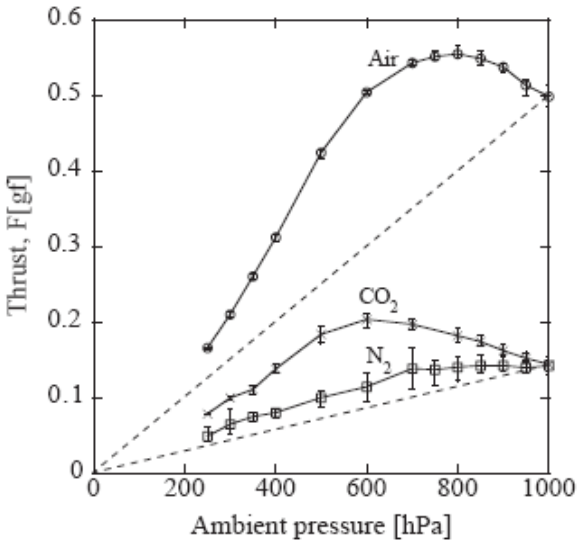

Figure 3.7. Thrust produced by the plasma actuator as a function of working gas and pressure. The fact that the actuator is more efficient in air and carbon dioxide than in pure nitrogen suggests that the formation of negative ions play a significant role in the force production [10].

3.2 Experiments

Experiments are usually set up using a signal generator, an amplifier, an impedance matching network and a transformer [7, 8, 15-17]. The signal generator produces an AC waveform of a few volts in the frequency range of a few kilohertz. Amplifiers used are usually high power audio amplifiers designed for Public Adress (PA) systems, these amplifiers can produce up to 100 V output into a few ohm loads. To drive the plasma actuator the signal has to be transformed up to a few kilovolts by means of a transformer, see Figure 3.8. Some researchers also include an impedance matching network between the amplifier and the transformer. Other researchers, with larger budgets, drive the plasma actuator directly by means of a laboratory grade high voltage amplifier [10].

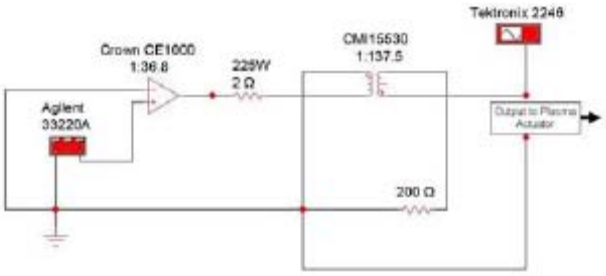

Figure 3.8. Illustration of the experimental setup used by M. L. Post *et al*. [15]. An Agilent signal generator provides the input signal to a Crown CE1000 PA amplifier (1 kW output power) connected to a high voltage step up transformer that drives the plasma actuator. No impedance matching network is used in this particular setup.

3.2.1 Dielectric materials

The dielectric material used by most researchers is a Kapton™ (Polyimid) foil or tape, this choice is primarily due to the very high temperature resistance and dielectric strength of this material [6, 7, 9, 10, 17, 20]. A typical Polyimid film tape has a film thickness of 0.03 mm and a dielectric strength of about 7.5 kV, the temperature range is -73 to 260°C. When a dielectric is subjected to large alternating electric fields power is lost due to heating of the dielectric. Roth and Dai investigated the effect of power loss due to dielectric heating and tabulated the results [6], see Table 2. The figure of merit is the dielectric loss factor, $\varepsilon_r \tan\delta$, where ε_r is the relative dielectric constant of the medium and $\tan\delta$ is called the *loss tangent* and is a measure of the insulating properties of the medium, it is defined as

$$\tan\delta = \frac{\sigma}{\omega\varepsilon_0\varepsilon_r} \tag{30}$$

where ω is the frequency of the applied electric field and σ is the conductivity of the material. The average power dissipated per unit volume is

$$p = \frac{1}{2}\mathbf{J}\cdot\mathbf{E} = \frac{1}{2}\sigma\mathbf{E}^2 = \frac{1}{2}\omega\varepsilon_0\varepsilon_r \tan\delta\,\mathbf{E}^2 \tag{31}$$

The total power loss due to dielectric heating is by integrating equation 31 over the volume of the dielectric

$$p = \frac{1}{2}\iiint \omega\varepsilon_0\varepsilon_r \tan\delta\,\mathbf{E}^2\, dV\,. \tag{32}$$

The volume of dielectric needed is inversely proportional to its dielectric strength this imply that a relatively lossy material can be a better choice than a low loss material provided that it has a high dielectric strength. The dielectric featuring the highest dielectric strength is Kapton, a trade mark of DuPont industries. Kapton exists in many different varieties and it is not clear which kind of Kapton that was used in the study by Roth *et al.*, specifically DuPont manufacture Kapton foils especially designed to withstand corona discharges without being damaged (Kapton CR). These foils are extensively used in high voltage transformers and other high voltage equipment where partial discharges may cause problems for other dielectric materials.

Table 2. Characteristics of various dielectric materials [6].

Material	**Mass density [kg/m^2]**	**Dielectric constant**	**Dielectric strength [MV/m]**	**Dielectric loss factor ε_r tanδ**	**Reference**
Teflon™	2160	2,1	11,2	0,00021	DuPont
Quartz	2200	5	25	0,00005	CEVP Ltd.
Aluminum Oxide	3700	9,4	15	0,00376	KYOCERA
Glass	2600	3,8	10	0,0152	matWeb
Lexan™	1190	2,9	16	0,02465	GE Plastic
Mica	2800	4~9	25	0,0052~0,0117	McMaster
Pyrex® glass	2530	4,1	15	0,0205	Corning
PC board	1690	5	16,8	0,025	DuPont
Bakelite	1420	5~22	24	0,1~0,44	MatWeb
Kapton™	1420	3,5	154	0,0315	DuPont
Garolite® G10	1820	5,2	20	0,025	K-mac plastics
Garolite® G7	1680	4,2	15	0,003	K-mac Plastics

In aerospace applications the density of the material is also of crucial importance. Roth *et al*. concludes that, the power loss due to dielectric heating can be of the same magnitude as the power spent to maintain the plasma and that, in terms of induced flow velocity divided by power in, the best materials are quartz and Teflon. However, this study uses materials of different thickness so the geometry varies with material and it is not clear that the conclusion by Roth *et al*. will hold in a case where the geometry is not allowed to change.

3.2.2 Electrode materials and geometry

Very little has been done so far in order to examine the effect of different electrode materials or electrode geometries. Studies have been made where the distance between the top and bottom electrodes have been altered, both by varying the thickness of the dielectric and by changing the lateral distance between the top and bottom electrodes but very little effort have been spent on investigating the effect of different electrode shapes. The parametric study by Takashi Abe *et al*. does however include an experiment performed with a stainless steel mesh-like top electrode [10]. The reason for using this type of electrode is that, for a given applied electrode voltage, the electric field close to the electrode surface will be stronger than in the case of a simple foil electrode. The same study also includes experiments with foil electrodes of different thickness and it was found that the plasma actuator became more efficient when the thickness of the foil was decreased. It was also found that the mesh-electrode was about 50 % more efficient than a foil electrode of the same thickness.

Figure 3.9. Stainless steel mesh electrode used by Takashi Abe *et al.* in order to enhance the electric field close to the electrode surface and obtain a higher density of ions. This method proved to be about 50 % more efficient than using a simple metal foil of the same thickness. The thickness of the mesh is 25 µm.

It was shown by Enloe *et al*. that a stronger electric field (for the same applied voltage) creates a more efficient actuator [24]. The electric field can be increased without changing the applied voltage by changing the geometry of the electrodes, either by moving them closer together or by changing the shape of the electrodes in the way done by Takashi Abe *et al*. [10].

3.2.3 Applications and actuator geometry

Although most experimentalists have been concerned with linear actuators designed to be applied in the spanwise direction of an airfoil experiments on other geometries have also been performed. Santhaakrishnan *et al*. investigates three different geometries, two circular and one linear [17].

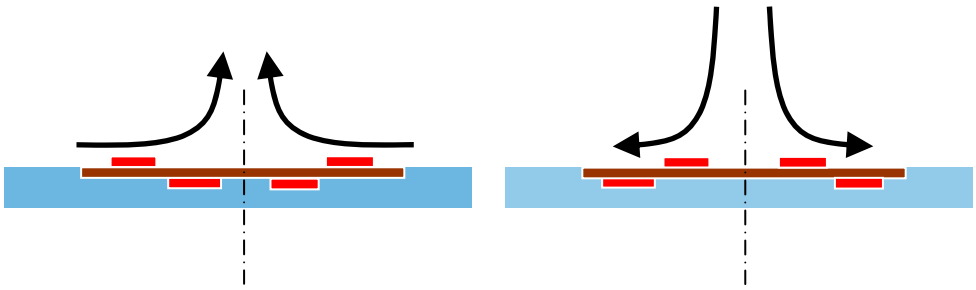

Figure 3.10. Two different cylindrically symmetric geometries used by Santhaakrishnan *et al.* to trip the boundary layer [17]. Arrows indicate the direction of induced flow. Note that both geometries can be used either in a cylindrically symmetric geometry to create cylindrical jets or in a linear geometry to create linear jets.

It was found that the cylindrical plasma actuator produced a wall jet comparable to jets produced by more conventional mechanical systems using oscillating diaphragms. Rahel *et al*. investigated other, more complex geometries, to create pumps with no moving parts and jets normal to the actuator surface [25]. The circular configuration of Figure 3.10 can be modified to generate a larger net flow by creating a star like geometry, see Figure 3.11.

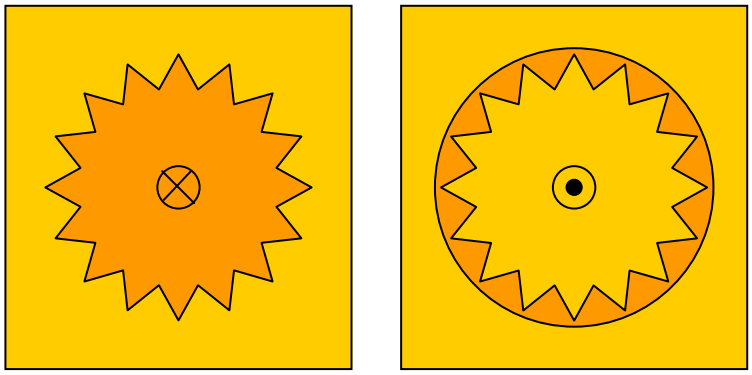

Figure 3.11. . Illustration of star like configuration. Because of the longer boundary this configuration generates more momentum than a purely circular one. Arrow indicates direction of flow at centre of actuator. The geometry to the left will create an inflow of gas at the centre and an outflow at the boundary. The geometry to the right will work in the opposite direction sucking gas along the plane in towards the middle where it is forced to move upwards (out of the paper) and create a circular jet.

An axial pump with no moving parts can be created by placing the actuator in a spiral on a dielectric tube as illustrated in Figure 3.12. Since it is only the air close to the inner surface of the cylinder that is affected, the cylinder must be long in comparison to its radius. The outer electrode must be covered by a dielectric so that it does not come in contact with surrounding gas.

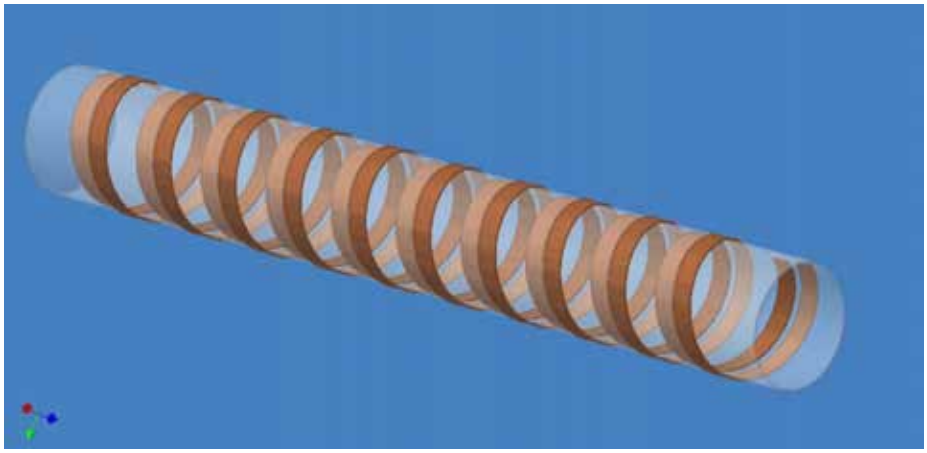

Figure 3.11. Illustration of tubular plasma generator acting as a linear pump with no moving parts, after Rahel *et al*. [25].

3.2.4 Wind tunnel experiments

Most of the experiments performed in wind tunnels aim at increasing the stall angle for a given airfoil at velocities in the range 10-75 m/s [7, 18-21]. Orlov *et al*. managed to increase the stall angle on an NACA 0021 airfoil using leading edge mounted plasma actuators by 5 degrees, from 17º to 22º at free speeds up to 30 m/s and chord Reynolds numbers of $2 \cdot 10^5 – 6 \cdot 10^5$. In this study the plasma actuators are driven in an ‘unsteady mode’ using short duty cycles (10 %) thus creating an actuator that uses 90 % less energy than one that is operated at full duty cycle. Opaits *et al*. investigated the NACA 0015 airfoil at free stream velocities between 20 m/s and 75 m/s. At 20 m/s they

increased the stall angle from 15º to 19º, at 44 m/s the stall angle was increased from 15º to 18º and at 75 m/s they managed to keep the flow attached up to 21º using two, instead of one, actuators. Most of the studies on separation control show similar results, what is lacking are experiments in higher free stream velocities, Opaits *et al.* showed that the concepts is useful up to about 75 m/s, but we have been unable to find any reports on experiments at higher speeds.

Labergue *et al.* used the plasma actuator to promote separation over a hinged end plate by placing an actuator so that it created an opposing flow with respect to the free stream flow [22]. The experimental setup is illustrated in Figure 3.13, free stream speeds between 5 and 30 m/s were used. Reynolds numbers varied between 3300 and 20000, based on the length Lb, see Figure 3.13. In these experiments a comparison between a DC discharge and an AC (DBD) discharge was made and it was found that the AC (DBD) discharge outperformed the DC discharge. This was attributed to the difficulty of creating a stable and homogenous DC discharge. Labergue *et al.* finishes by emphasizing the need of experiments at higher free stream velocities and promises to return with a new paper including experiments at up to 80 m/s free stream velocity.

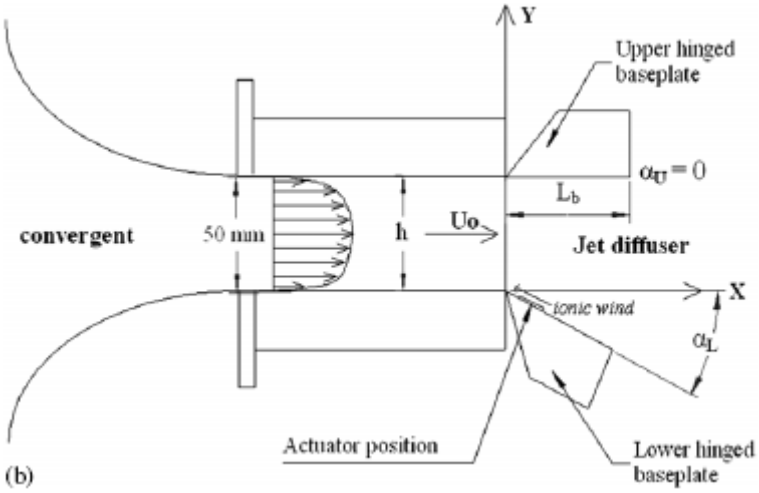

Figure 3.13. Illustration of the experiment performed by Labergue *et al.* The purpose was to create separation by placing the actuator so that it induced a boundary flow opposing the free field flow. In these experiments separation was achieved at free stream velocities up to 30 m/s, higher free stream velocities was not tested.

Thomas *et al.* investigated the use of plasma actuators for bluff body flow control [20]. Using several plasma actuators placed around a cylinder at Reynolds number Re_D=33000, they managed to delay separation and unsteady vortex shedding, see Figure 3.14. Karman shedding was totally eliminated, turbulence levels in the wake decrease significantly and the near field sound pressure was reduced by 13.3 dB.

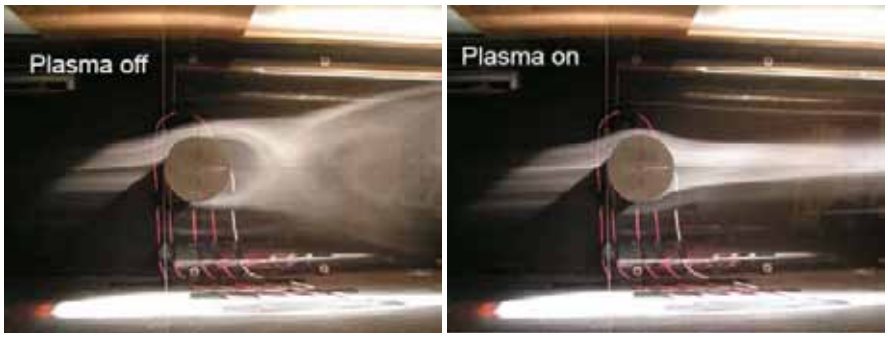

Figure 3.14. Experiments by Thomas *et al.* on bluff body flow control [20]. Cylinder In cross flow at ReD=33000 showing strong separation with no flow control (left) and an attached boundary layer with plasma actuators turned on (right).

In these experiments Thomas *et al.* used four plasma actuators placed around the cylinder at ±90º and ±135º with respect to the direction of the incoming flow. They used both steady (100 % duty cycle) and unsteady actuation (at 25 % duty cycle) and found that unsteady actuation was, in fact, even more effective than steady actuation. Turbulence level was decreased by 50 % using 100 % duty cycle and by 66 % using a 25 % duty cycle. This result seems to indicate that it is not only a waste of energy to use steady actuation; it is in fact counterproductive.

Surprisingly few researchers have investigated the influence of a plasma actuator on skin friction drag by placing one or several actuators on a flat plate in a wind tunnel. Most researchers do mention a reduction in skin friction drag as a goal for the development of the plasma actuator but do not publish such data, instead they publish data on increased stall angle as improved lift to drag ratios. Roth *et al.* did early experiments on skin friction drag in 1998 and found that it could be reduced by a factor of 7 at low free stream speeds of 7 m/s [13]. The effect decreased with increasing free speed velocity and at 15 m/s the drag reduction was only a factor of 1.25 and at 20 m/s the effect was not measurable. It should be noted here that these experiments were performed almost five years before the real development of actuator geometry took of and could probably be improved upon using up to date geometries and power supplies.

Plasma actuators instead of traditional moving flaps and slats was investigated by Corke *et al.* [23]. Two spanwise arrays of plasma actuators were placed on the suction side of a NACA 0015 airfoil, one on the leading edge and one close to the trailing edge of the airfoil. The spanwise length of the actuators was 30 cm. The actuators resulted in an increase in both C_{Lmax} and maximum stall angle and a 340 % improvement of lift to drag ratio (C_L/C_D). The electrical power to the actuator was no more than 2 W, meaning that the electrical power per spanwise meter of wing was about 2/0.3 = 6.7 W/m. The trailing edge actuator was found to produce the same result as a plane trailing edge flap. A slight decrease in minimum C_D was also noticed in these experiments.

3.3 Modelling

In order to impedance match the power supply to the plasma actuator several attempts at modeling the discharge as consisting of lumped circuit elements has been made. The simplest approaches assume that the actuator can be modeled by three capacitors and a discharge as shown in Figure 3.15. Capacitor C1 represents the capacitance between the electrodes due to the coupling through the dielectric alone. Capacitor C2 represents the capacitance between the buried (right electrode in Figure 3.2) electrode and the plasma.

Capacitor C3 represents the capacitance between the upper (left) electrode and the upper dielectric surface. The current generator, Ig, represents the plasma itself and the current through this device is related to the applied voltage through an exponential expression according to,

$$I = \begin{cases} 0, \text{for} \, U_g < U_{breakdown} \\ \alpha\left(U_g - U_{breakdown}\right)^{\beta}, \text{for} \; U_g \geq U_{breakdown} \end{cases} \tag{33}$$

where U_g is the voltage across the plasma (gap), $U_{breakdown}$ is the breakdown voltage of the gap, α is a constant that depends the size of the discharge (electrode distance and length of actuator) and β is an integer that may range from 1 to 12 depending on the discharge mode of the actuator [26].

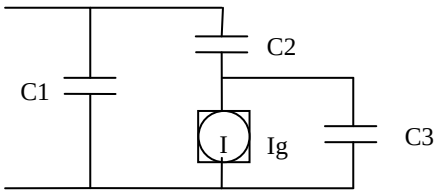

Figure 3.15. Lumped circuit equivalent of plasma actuator. Capacitor C1 represents the capacitance between the electrodes due to the coupling through the dielectric alone. Capacitor C2 represents the capacitance between the buried (right electrode in Figure 3.2) electrode and the plasma. Capacitor C3 represents the capacitance between the upper (left) electrode and the upper dielectric surface. The current generator, Ig, represents the plasma itself and the current through this device is related to the applied voltage through an exponential expression, see Equation (33). Some researchers use a varying resistance in place of the current generator [27].

More advanced models take into account the propagation of the surface plasma across the buried electrode so that the resistance and capacitance of the plasma varies in time [19].

3.4 Simulation

3.4.1 Introduction

When performing the literature search for computational papers in this area, our prime concern was to identity the simplest possible models which contain the fundamental mechanisms of plasma dynamics and its interaction with the fluid. Then it turned out that a large number of scientific papers are devoted to the study of models only incorporating one (positive) type of ion. This, in spite of the argument presented in Section 2.6 which include negative ions as important for the process.

In this section we will present the simpler model, with only positive ions, since it has been used fairly extensively in ongoing research world-wide. The articles included in this survey differ, at least concerning details, for the models they study. We will mostly follow [28] below, and comment how the models in the other papers relate to this one. We will also briefly comment on the numerical methods used for the solution of these

partial differential equations and give some examples of the computational geometries studied and computed quantities of interest.

In [28] two different geometrical configurations of a DBD are simulated in two space dimensions. These configurations are simplified. The physical model includes three species (neutrals, electrons and positive ions) and is described below. The gas is taken to be helium and this is motivated by the claim that ”its plasma coefficients and chemistry are known”.

3.4.2 Governing equations

Here we describe the physical model used in [28]. The charge conservation is expressed by the following two equations for the electron and ion densities respectively. On the left hand side is the material rate of change of charge and on the right hand side are the ionization and recombination terms.

$$\frac{\partial n_e}{\partial t} + \nabla \cdot \left(n_e \boldsymbol{v}_e \right) = \alpha n_e - \beta n_e n_i \qquad \text{(electrons)(34)}$$

$$\frac{\partial n_i}{\partial t} + \nabla \cdot \left(n_i \boldsymbol{v}_i \right) = \alpha n_e - \beta n_e n_i \qquad \text{(ions) (35)}$$

Compared to the model given in Section 2.6, we see that the photo-ionization is neglected here. Since we only have three species, we can drop the indices on the coefficients for ionization and recombination.

The electron and ion velocities are given by the following expressions where the first term represents the electric field force (V is the electric potential) and the second represent diffusion.

$$\boldsymbol{v}_e = \mu_e \nabla V + \frac{D_e}{n_e} \nabla n_e \qquad (36)$$

$$\boldsymbol{v}_i = -\mu_i \nabla V + \frac{D_i}{n_i} \nabla n_i \qquad (37)$$

The electric potential is determined by a Poisson equation with the electric charge in the right hand side.

$$\nabla \cdot \left(\varepsilon \nabla V \right) = e\left(n_e - n_i \right) \qquad (38)$$

Inserting (36) and (37) in (34) and (35) respectively, we see that the model consists of two convection-reaction-diffusion equations (one for electrons and one for ions). These are coupled with the Possion equation for the electric potential. The three ”primary” unknows are thus n_e, n_i and V. We also note that these equations can be solved completely independently of the gas flow equations. The simplest way to couple these equations to the flow equations would be to include the velocity relative to the neutral phase in equations (36) and (37) instead of the absolute velocities, i.e. for the electrons, the following equation

$$\boldsymbol{v}_e - \boldsymbol{v}_n = \mu_e \nabla V + \frac{D_e}{n_e} \nabla n_e \qquad (36')$$

The complexity of this three equation model is to a large extent determined by the (non-linear) coefficients for ionization, recombination, mobility etcetera. We believe that the results are quite sensitive to the expressions used for these coefficients and furthermore their modelling (at least for some of the coefficients) is a subject of research. We discuss the plasma coefficients more in Section 2.6.

The boundary conditions only briefly mentioned in [28]. The geometry consists of two electrodes (one exposed and one embedded in the dielectric) and two regions with gas and dielectrics respectively. The electrical potential is given, as a function of time, on the electrodes. At the exposed electrode, the electron flux "is based on the electron thermal velocity and is neglected unless directed toward the wall". For the other unknowns and the other boundaries (including outer boundaries), homogeneous Neumann conditions are used. There should be no particular difficulty with the "artificial" outer boundary conditions since the charge densities are very low there.

The fluid flow equations are very briefly described in [28], and it would seem that the description is not complete. The helium gas is modelled as an ideal (compressible) gas. The only influence of the plasma in the flow equations is the following force term in the momentum equation.

$$\mathbf{f}_p = \varpi e\left(n_i - n_e\right)\nabla V \tag{39}$$

This term may be the crudest approximation in the model presented here. The only comment in the paper [1] is: "The factor ϖ is introduced to modulate the effect of electric field". No value or expression for the factor is given. Furthermore, no energy equation is given in [28] for the gas flow. The energy equation is necessary if the compressibility effects are to be taken into account. From the several remarks in [28] it would seem that they use compressible gas dynamics. In this parameter range, and with this level of approximation, it however should be adequate to treat the fluid as incompressible.

The program which is used for the solution of the above equations is referred to as "the multiscale ionized gas (MIG) flow code". It is based on the finite element method and is said to be described in papers [29] and [30]. Atypical simulation which is reported in [28] uses a mesh 51x53=2703 quadrilateral elements, some of which has an aspect ratio as large as 90. Considering the strong gradients in the charge densities it seems to be questionable if this mesh has sufficient quality and refinement to give accurate solutions.

3.4.3 Plasma coefficients

Here we will give additional information, based on [28], about the plasma coefficients which enter the model expressed by equations (34)-(38).

The electron mobility is given by the following expression, which involves constants.

$$\mu_e = \frac{e}{m_e \nu_{en}} \tag{40}$$

Here e is elementary charge, m_e is the electron mass and $\nu_{en} \approx 10^{12}\ s^{-1}$ is the electron-neutral collision frequency. The electron diffusion is given by,

$$D_e = \frac{T_e \mu_e}{e}, \qquad (41)$$

where T_e is the energy (temperature). It is not clear from [28] if the electron energy is assumed constant. The ion mobility is given by analytical expressions in terms of E/p, compare the discussion in section 2.6 where it is noted that the mobility should be a function of the reduced electric field strength. The ion diffusivity is not given in [28].

The ionization rate is given by the expression

$$\alpha = A \exp\left(-\frac{B}{(E/p)^{0.4}} \right) p \mu_e E \ \ \mathrm{s}^{-1} \qquad (42)$$

where A=4.4 $\mathrm{cm^{-1}Torr^{-1}}$ and B=14 $(\mathrm{V/(cmTorr)})^{0.4}$. Finally, for the recombination rate, it is only said in [28] that it is given by an expression of the form,

$$\beta = V_{eth} \sigma_{ei}(V_{eth}), \qquad (43)$$

where V_{eth} is the electron thermal velocity and σ_{ei} is the electron ion collision cross section. These coefficients together with equations (34)-(38) and the boundary conditions constitutes a complete model for the plasma flow. We see that there remains some information, not given in [28], concerning coefficients and boundary conditions to completely specify the model.

3.4.4 Other simulation models in the literature

Here we give a brief overview of other related models and simulation methods which have been studied in relation to plasma flow control. The main source for this is the conference proceedings of the main, yearly, AIAA conference.

In one type of study, the focus is on the fluid dynamics, and the plasma effects are only modelled as a force term in the gas momentum equation. This of course implies a very crude description of the plasma dynamics. This approach is used in e.g. [31] where a plasma actuator on a realistic (two-dimensional) airfoil is studied. The lift of the air-foil is also optimized with respect to a number of parameters including the DBD excitation frequency. The program used is called CFD3D and has been developed at NASA. It implements the finite volume method.

When partial differential equations for the charge densities are used to model the plasma dynamics, there are many different levels of refinement in the models used. The paper [32] uses a three (electron, positive ion, neutral) species model as that described in [28] and above. In [33] negative ions are also included, yielding a four species model. In [34], five species are included and in [35] as many as nine species are modelled with separate convection-diffusion-reaction equations. All of these papers study simple rectangular configurations for the plasma actuator, and the computations use relatively few finite elements or finite volume cells.

A wide range of different numerical methods have been applied. In papers [28] and [35] the finite element method (FEM) is used. In some papers it is not clear if the finite

difference method (FDM) or the finite volume method has been used (FVM) it is only specified which scheme is used to discretise the convective term. Such schemes (flux-corrected transport, FCT, for example) can however be adapted both to a FDM and a FVM framework, furthermore there are many ways to generalise these schemes to systems of equations and several space dimensions. All publications in our list of references report simulations with two space dimensions.

4 References

1. Roth, J.R., *Physics and phenomenology of plasma actuators for control of aeronautical flows.* Journal of Physics D, 2007. **40**.
2. Larsson, A., *Inhibited Electrical Discharges in Air*, in *Faculty of Science and Technology 12*. 1997, Uppsala University: Uppsala.
3. G E Georghiou, *et al*., *Numerical modelling of atmospheric pressure gas discharges leading to plasma production.* Journal of Physics D, Applied physics, 2005. **38**.
4. I. A. Kossyi, *et al*., *Kinetic scheme of the non-equilibrium discharge in nitrogen-oxygen mixtures.* Plasma Sources Sci. Technology, 1992. **1**(3): p. 207-220.
5. Arvind Santhanakrishnan and J.D. Jacob, *Flow control with plasma synthetic jet actuators.* Journal of Physics D, 2007. **40**.
6. J. Reece Roth and X. Dai. *Optimization of the Aerodynamic Plasma Actuator as an Electrohydrodynamic (EHD) Electrical Device*. in *44th AIAA Aerospace Sciences Meeting and Exhibit*. 2006. Reno, Nevada.
7. Karthik Ramakumar and J.D. Jacob. *Flow Control and Lift Enhancement Using Plasma Actuators*. in *35th AIAA Fluid Dynamics Conference and Exhibit*. 2005. Toronto, Ontario, Canada.
8. Mehul P. Patel, *et al*. *Scaling Effects of an Aerodynamic Plasma Actuator*. in *45th AIAA Aerospace Sciences Meeting and Exhibit*. 2007.
9. R. Rivir, *et al*. *AC AND PULSED PLASMA FLOW CONTROL*. in *42nd AIAA Aerospace Sciences Meeting and Exhibit*. 2004. Reno, Nevada.
10. Takashi Abe, *et al*. *A Parametric Experimental Study for Momentum Transfer by Plasma Actuator*. in *45th AIAA Aerospace Sciences Meeting and Exhibit*. 2007. Reno, Nevada.
11. Chen, Z., *Impedance Matching for One Atmosphere Uniform Glow Discharge Plasma (OAUGDP) Reactors.* IEEE transactions on Plasma Science, 2002. **30**(5).
12. Roth, J.R., *Industrial Plasma Engineering*. Vol. 2. 2001: IOP.
13. J.Reece Roth, Daniel M. Sherman, and S.P. Wilkinson. *BOUNDARY LAYER FLOW CONTROL WITH A ONE ATMOSPHERE UNIFORM GLOW DISCHARGE SURFACE PLASMA*. in *36th Aerospace Sciences Meeting and Exhibit*. 1998. Reno, Nevada.
14. G. I. Font, *et al*. *Plasma Discharge Characteristics and Experimentally Determined Boundary Conditions for a Plasma Actuator*. in *45th AIAA Aerospace Sciences Meeting and Exhibit*. 2007. Reno, Nevada.
15. Martiqua L. Post, *et al*. *Effects of an Aerodynamic Plasma Actuator on an HSNLF Airfoil*. in *45th AIAA Aerospace Sciences Meeting and Exhibit*. 2007. Reno, Nevada.
16. James W. Gregory, *et al*. *Force Production Mechanisms of a Dielectric-Barrier Discharge Plasma Actuator*. in *45th AIAA Aerospace Sciences Meeting and Exhibit*. 2007. Reno, Nevada.

17. Arvind Santhanakrishnan, Jamey D. Jacob, and Y.B. Suzen. *Flow Control Using Plasma Actuators and Linear/Annular Plasma Synthetic Jet Actuators*. in *3rd AIAA Flow Control Conference*. 2006. San Francisco, California.

18. D.F. Opaits, *et al*. *PLASMA CONTROL OF BOUNDARY LAYER USING LOW-TEMPERATURE NON-EQUILIBRIUM PLASMA OF GAS DISCHARGE*. in *43rd AIAA Aerospace Sciences Meeting and Exhibit*. 2005.

19. Dmitriy M. Orlov, *et al*. *Modeling and Experiment of Leading Edge Separation Control Using SDBD Plasma Actuators*. in *45th AIAA Aerospace Sciences Meeting and Exhibit*. 2007. Reno, Nevada.

20. Flint O. Thomas, Alexey Kozlov, and T.C. Corke. *Plasma Actuators for Bluff Body Flow Control*. in *3rd AIAA Flow Control Conference*. 2006. San Francisco, California.

21. J. Reece Roth, *et al*. *SUBSONIC PLASMA AERODYNAMICS USING LORENTZIAN MOMENTUM TRANSFER IN ATMOSPHERIC NORMAL GLOW DISCHARGE PLASMAS*. in *55thAPS Gaseous Electronics Conference*. 2002.

22. A Labergue, *et al*., *Separation control using plasma actuators: application to a free turbulent jet.* Journal of Physics D, 2007. **40**.

23. Thomas C. Corke, Chuan Hey, and M.P. Patel. *PLASMA FLAPS AND SLATS: AN APPLICATION OF WEAKLY-IONIZED PLASMA ACTUATORS*. in *2nd AIAA Flow Control Conference*. 2004. Portland, Oregon.

24. C. L. Enloe, *et al*., *Mechanisms and Responses of a Single Dielectric Barrier Plasma Actuator: Geometric Effects.* AIAA Journal, 2004. **42**.

25. Jozef Rahel, J. Reece Roth, and X. Dai. *Three-Dimensional Flow Acceleration Using Plasma Aerodynamic Actuators*. in *56th Annual GEC*. 2003. San Francisco.

26. Zhiyu, C., *PSPICE Simulation of One Atmospheric Uniform Glow DIscharge Plasma (OAGDP) Reactor Systems.* IEEE Transactions on Plasma Science, 2003. **31**(4): p. 511-520.

27. C. L. Enloe, *et al*., *Mechanisms and Responses of a Single Dielectric Barrier Plasma Actuator: Plasma Morphology.* AIAA Journal, 2004. **42**(3).

28. Subrata Roy and D.V. Gaitonde, *Force interaction of high pressure glow discharge with fluid flow for active separation control.* Physics of Plasmas, 2006. **13**.

29. Subrata Roy, *et al*., *Modeling low pressure collisional plasma sheath with space-charge effect.* Physics of Plasmas, 2003. **10**(6).

30. Dinesh Balagangadhar and S. Roy, *Design sensitivity analysis and optimization of steady fluid-thermal systems.* Comptational Methods Appl. Mech., 2001. **190**: p. 5465.

31. Thomas C. Corke, Benjamin Mertz, and M.P. Patel. *Plasma Flow Control Optimized Airfoil*. in *44th AIAA Aerospace Sciences Meeting and Exhibit.* 2006. Reno, Nevada, USA.

32. Poggie, J. *Numerical Simulation of DC and RF Glow Discharges.* in *45th AIAA Aerospace Sciences Meeting*. 2007. Reno, Nevada.

33. A. V. Likhanskii, *et al*. *Optimization of Dielectric Barrier Discharge Plasma Actuators Driven by Nanosecond Pulses*. in *45th AIAA Aerospace Sciences Meeting and Exhibit*. 2007. Reno, Nevada.

34. J.-C. Matéo-Vélez, *et al*. *NUMERICAL MODELLING OF CORONA DISCHARGES AND THEIR INTERACTION WITH AERODYNAMICS.* in *EUCASS 2005*. 2005.

35. Subrata Roy, K.P. Singh, and D.V. Gaitonde. *Air Plasma Actuators for Effective Flow Control*. in *45th AIAA Aerospace Sciences Meeting and Exhibit*. 2007. Reno, Nevada.